Electronic transition in $La_{1-x}Sr_xTiO_3$

C. C. Hays,* J.-S. Zhou, J. T. Markert, and J. B. Goodenough
Texas Materials Institute, ETC 9.102, University of Texas at Austin, Austin, Texas 78712-1063
(Received 21 May 1999)

The transition with increasing x in $La_{1-x}Sr_xTiO_3$ from an antiferromagnetic, *p*-type polaronic conductor to an *n*-type metal with an enhanced Pauli paramagnetism was investigated by monitoring changes in structure, magnetic properties, and, under different hydrostatic pressures, the resistance and thermoelectric power of ceramic samples. We conclude that $LaTiO_3$ is an itinerant-electron antiferromagnet and the transition is first order with a phase separation associated with cooperative oxygen-atom displacements that segregate strongly correlated states from Fermi-liquid states. The Néel temperature $T_N \approx 145$ K decreases precipitously to 100 K at the phase limit $x = 0.045 \pm 0.005$; the two-phase domain extends over the compositions $0.045 \leqslant x \leqslant 0.08$. [S0163-1829(99)04638-X]

I. INTRODUCTION

Following an early mapping of the localized versus itinerant electronic behavior of the single-valent transition-metal oxides with perovskite structure,[1] Greedan and co-workers[2–8] undertook a systematic study of the $R_{1-x}TiO_3$ perovskites, with R a lanthanide or yttrium atom. These perovskites are all orthorhombic, *Pbnm*, due to a room-temperature geometric tolerance factor $t = (R\text{-O})/\sqrt{2}(\text{Ti-O}) < 1$ for the ideal structure.[2] The resulting compressive stress in the (Ti-O) bond length is relieved by a cooperative rotation of the $TiO_{6/2}$ octahedra about the [110] axis of the orthorhombic structure. These rotations bend the Ti-O-Ti bond angle to (180°-ϕ), and ϕ increases with decreasing atomic radius of the R^{3+} ion. Within the $(TiO_3)^{3-}$ array, the (180°-ϕ) Ti-O-Ti interactions control the electronic properties, and the strength of these interactions decreases with increasing ϕ.[1]

Greedan's initial objective was to explore the change in physical properties of the single-valent $(TiO_3)^{3-}$ array on going from an itnerant-electron, Pauli paramagnet in metallic $LaTiO_3$ to a ferromagnetic $(TiO_3)^{3-}$ array in $YTiO_3$.[4] However, the earlier work on $LaTiO_3$ lacked sufficient control of the oxygen stoichiometry. Stoichiometric $LaTiO_3$ is an antiferromagnetic insulator ($T_N \approx 140$ K) with a weak, canted-spin ferromagnetic moment due to an antisymmetric exchange contribution $\mathbf{D}_{ij} \cdot \mathbf{S}_i \times \mathbf{S}_j$ with $\mathbf{D}_{ij}$ parallel to the b axis. The metallic, Pauli paramagnetic phase was $LaTiO_{3+\delta}$ with $\delta > 0.02$, and since there is no place in the structure for interstitial oxygen, this phase is more correctly designated $La_{1-x}Ti_{1-x}O_3$. This finding frustrates investigation of the transition from a Pauli paramagnetic metal to a magnetically ordered insulator in a single-valent $(TiO_3)^{3-}$ array, but it permits study of the transition from itinerant-electron antiferromagnetism in stoichiometric $LaTiO_3$ to a ferromagnetic $(TiO_3)^{3-}$ array containing more localized electrons in $GdTiO_3$ to $LuTiO_3$ and in $YTiO_3$.[3–5]

The spin-$\frac{1}{2}$ character of a localized Ti(III) configuration and the change from antiferromagnetic insulator to Pauli paramagnetic metal on oxidation to a mixed-valent state is clearly analogous in a three-dimensional (3D) array to what happens in a 2D CuO_2 sheet of the high-T_c copper-oxide superconductors. Motivated by this analogy, Tokura and co-workers[9–18] have used to great advantage their ability to grow quality $R_{1-x}A_xTiO_3$ single crystals (A = alkaline earth) to explore the transition from a Mott-Hubbard insulator in a single-valent $RTiO_3$ parent compound to a mixed-valent, Pauli paramagnetic metal with oxidation of the $(TiO_3)^{(3-\eta)-}$ array, $0 \leqslant \eta \leqslant 1$. The critical oxidation parameter η_c for the transition increases progressively with the Mott-Hubbard energy gap $E_g \approx U - W$ of the parent $RTiO_3$, where U is the on-site electron-electron energy required to add a second electron to a d^1 configuration and W is the width of the π^* conduction band. The energy gap estimated from the onset of the optical conductivity increases from about 0.2 eV in $LaTiO_3$ to 1.2 eV on approaching $YTiO_3$, and a calculated W decreases from about 2.45 to 2.05 eV.[17]

In this paper, we report the evolution of the stucture and magnetic susceptibility with Sr concentration x in $La_{1-x}Sr_xTiO_3$. In addition, we monitor the change with hydrostatic pressure in the temperature dependence of the resistance and thermoelectric power in the neighborhood of the critical oxygen parameter η_c.

II. EXPERIMENT

Polycrystalline $La_{1-x}Sr_xTiO_3$ specimens were prepared by arc melting in argon pelletized mixtures of stoichiometric quantities of La_2O_3 (99.99%) from GFS chemicals, Ti_2O_3, Ti (99.9%, 325 mesh) and $SrCO_3$ (99.99%) both from Johnson Matthey.[19] The Ti_2O_3 was prepared by reacting stoichiometric quantities of TiO_2 (99%) from Fisher Scientific and elemental Ti at 850 °C for at least 48 h in a sealed quartz tube evacuated to 10^{-5} Torr. The TiO_2 was heated at 800 °C in air prior to weighing. The La_2O_3 was heated to 1000 °C in air before weighing and mixing while still warm. The pellets were transferred quickly to the arc furnace to minimize contamination by moisture in the air. The melted pellets were inverted and remelted once to promote homogeneity. Arc-melted specimens with $0 \leqslant x \leqslant 0.8$ had a shiny black appearance. They were subsequently vacuum annealed in a sealed quartz tube for 48 h at 800 °C. X-ray diffraction with a Phillips powder diffractometer and Cu K_α radiation showed the

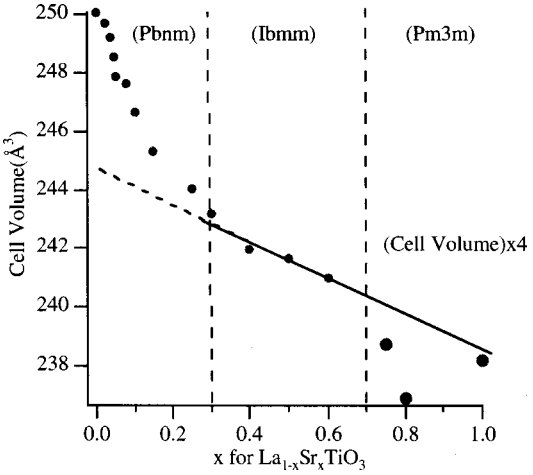

FIG. 1. Unit cell volume vs x for $La_{1-x}Sr_xTiO_3$.

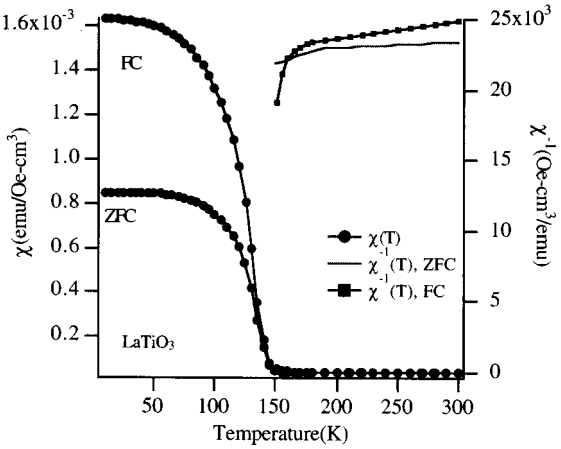

FIG. 2. Temperature dependence of magnetic susceptibility (ZFC and FC), $\chi(T)$, for $LaTiO_3$.

samples were single phase. The peak positions (2θ) were calibrated against a Si standard, and the lattice parameters were obtained with a least-squares fitting procedure. A Perkin-Elmer TGA-7 thermogravimetric analyzer (TGA) was used to determine the oxygen content from the weight gain on heating the samples in air to 1000 °C to oxidize all of the titanium to Ti^{4+}. The samples were oxygen stoichiometric within an experimental error of about 1% of the total oxygen content. Magnetic data were obtained from 10 to 300 K with a Quantum Design MPMS SQUID magnetometer in applied fields $-5 \leqslant H \leqslant 5$ T. The temperature dependence of the magnetic susceptibiltity, $\chi(T)$, and the field and time dependence of the magnetization $M(H)$ were recorded. The temperature dependence of the resistance $R(T)$ under different hydrostatic pressures was measured with the four-point probe method in a home-built device.[20] The thermoelectric power $\alpha(T)$ under different hydrostatic pressures was measured with an experimental device described elsewhere;[20] a temperature difference $\Delta T = 4$ K across the specimen was used for each measurement at ambient condition. The contribution to $\alpha(T)$ from the Cu leads was subtracted from all measurements.

III. RESULTS

A. Structure

In agreement with the literature,[2,21,22] the x-ray diffraction data showed a change in the space group of the system $La_{1-x}Sr_xTiO_{3\pm\delta}$ with increasing x from orthorhombic *Pbnm* to orthorhombic *Ibmm* at $x = 0.3$ and to the cubic $Pm3m$ structure at $x \approx 0.7$. Figure 1 shows the variation with x of the measured unit-cell volumes (multiplied by 4 for $Pm3m$). In the *Pbnm* phase, the increase in volume with decreasing x correlates with an increase in the electron effective mass m^* that has been observed in the metallic phase, and the jump in volume correlates with the opening of a Mott-Hubbard gap in the insulating phase.[11,13]

B. Magnetic studies

Figure 2 shows the temperature dependence of the magnetic susceptibility $\chi(T)$ for $LaTiO_3$ taken on heating in a magnetic field of 1 kOe after cooling in zero magnetic field (ZFC) and 1 kOe (FC). The observation of a weak, canted-spin ferromagnetism below a Néel temperature $T_N = 145$ K, somewhat higher than the $T_N = 130$ K reported by Goral, Greedan, and MacLean[4] and the $T_N = 138$ K reported by Tokura *et al.*,[13] indicates that the oxygen content was nearly stoichiometric. However, the inverse paramagnetic susceptibility, $\chi^{-1}(T)$, for the field-cooled (FC) run differs from that of the zero-field-cooled (ZFC) run; the ZFC run shows a change of slope near 190 K, which suggests either the onset of short-range magnetic order or a change in the character of the strong electron correlations below 190 K. This difference in the $\chi^{-1}(T)$ curves is unusual; it implies that cooling in a magnetic field influences the character of the paramagnetic state. The ZFC paramagnetic susceptibility is nearly temperature independent above 190 K, which is more typical of a strongly enhanced Pauli paramagnetism than of a Mott-Hubbard insulator. Fitting the FC curve to a Curie-Weiss law gives a Weiss constant $\theta < -1500$ K, which is uncharacteristic of a localized-electron paramagnetism. Nevertheless, the magnetic transition at T_N appears to be second order. Moreover, x-ray and neutron diffraction data[21,22] show that the room-temperature orthorhombic structure with $c/a > \sqrt{2}$ is retained at 10 K; there is no evidence of a cooperative spin-orbit coupling deformation below T_N expected for localized-electron antiferromagnetism. The data indicate, therefore, an itinerant-electron antiferromagnetism is stabilized in $LaTiO_3$.

Figure 3 compares the $M(H)$ hysteresis loops with $-50 \leqslant H \leqslant 50$ kOe at 10 K for ZFC and FC $LaTiO_3$. The FC loop has a smaller coercivity, a lower magnetization at 50 kOe, and a similar remanence $M_r \approx 0.225 \mu_B$/formula unit. The M_r value corresponds to a cant angle of $\theta = 13°$, where $\theta = 90°$ would correspond to ferromagnetic alignment of Ti(III) moments of $1\mu_B$. This minimum cant angle is large for antisymmetric-exchange canting; it indicates an important orbital-momentum contribution to the itinerant-electron exchange that is consistent with an unquenched orbital angular momentum for a localized Ti(III): t^1e^0 configuration in an octahedral site.

The observation[14] of a linear increase of T_N with hydrostatic pressure P would appear to be indicative of a localized-electron antiferromagnetism, but this relationship was origi-

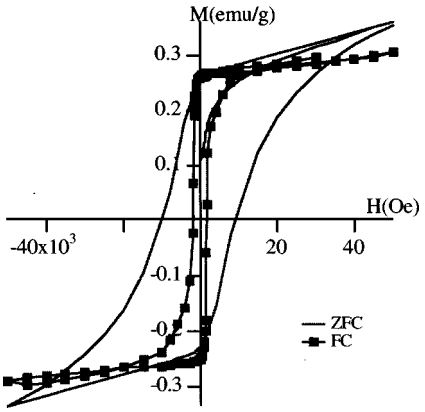

FIG. 3. Magnetization (ZFC and FC) loops at 10 K for $LaTiO_3$.

nally formulated[1] for the case of an orbitally nondegenerate system. Studies[4,10] of the system $La_{1-x}Y_xTiO_3$ have shown that narrowing the bandwidth W with increasing x lowers T_N until, at $x \approx 0.75$, there is a crossover to ferromagnetic order with a Curie temperature T_C that increases with x. Therefore the increase in T_N with pressure at $x=0$ may simply reflect an extrapolation of this dependence of T_N on W, a dependence that is due to a competition in an orbitally degenerate itinerant-electron band between intra-atomic–exchange stabilization of ferromagnetically coupled spins and interatomic bonding of spin-paired electrons. Increasing the Ti-O-Ti interatomic interactions with hydrostatic pressure, or broadening W chemically, increases the interatomic bonding favoring antiferromagnetic interactions at the expense of an intra-atomic–exchange stabilization of ferromagnetically coupled spins. Where there is an orbital degeneracy, a $dT_N/dP>0$ does not necessarily represent an increase in the superexchange interaction between localized spins, as is the case where there is no orbital degeneracy.

Figure 4 compares $\chi(T)$ curves taken on heating in 1 kOe after FC in 1 kOe for different compositions $La_{1-x}Sr_xTiO_3$; the range $0 \leqslant x \leqslant 0.075$ spans the metal-insulator (M-I) transition as well as the antiferromagnetic-paramagnetic transition. A precipitous drop with increasing x in both T_N and the 1 kOe magnetic moment at 4 K sets in at $x \approx 0.04$ (Fig. 5); but the drop in T_N stops at about 100 K in the range $0.05 \leqslant x \leqslant 0.08$, whereas the moment continues to decrease continuously to zero. This behavior is indicative of a first-order transition between an antiferromagnetic phase and a strongly correlated paramagnetic phase with an electronic phase segregation ocurring in the interval $0.04 \leqslant x \leqslant 0.08$. To what extent the hole-rich paramagnetic phase is associated with the Sr^{2+} ions or clusters is not known; short-range-cooperative oxygen-atom displacements can also induce the formation of multicenter hole-rich clusters that are mobile, as is illustrated in the manganese-oxide perovskites exhibiting a colossal magnetoresistance (CMR).[23] The mass-enhanced Pauli paramagnetism of the compositions $0.10 \leqslant x \leqslant 0.50$ have been well discussed by Tokura *et al.*[13] The apparently second-order transition at T_N may prove to be an order-disorder transition between clusters of strongly correlated electrons.

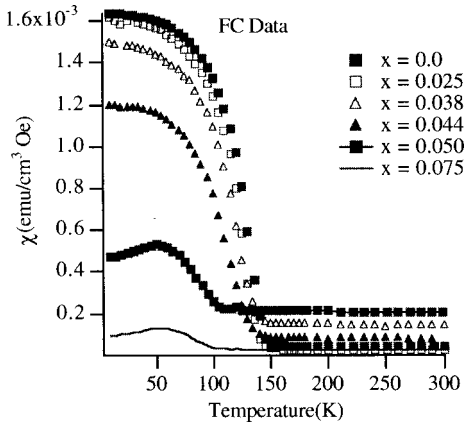

FIG. 4. Magnetic susceptibilty (FC), $\chi(T)$, for $La_{1-x}Sr_xTiO_3$ vs x.

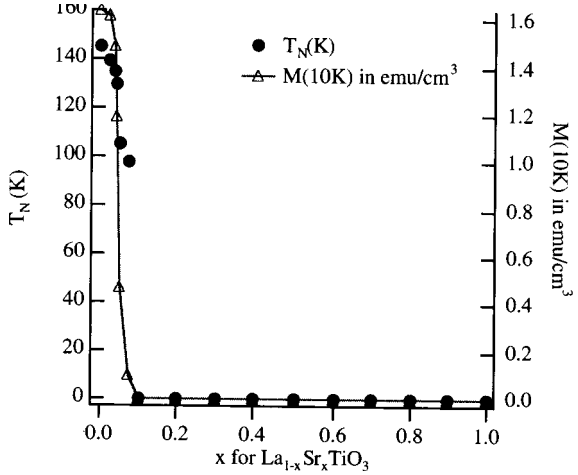

FIG. 5. Néel temperature, T_N, and magnetization at 10 K, $M(10\,\mathrm{K})$, for $La_{1-x}Sr_xTiO_3$ vs x.

Compositions in the range $0.05 \leqslant x \leqslant 0.08$ were studied further for evidence of two-phase and spin-glass behavior.[24] Four pertinent observations were made. (1) All samples showed a maximum in the ZFC $\chi(T)$ curves at a $T_a < T_N$ and a field-dependent $\chi(T)$ at $T < T_N$. The ZFC curves for $x=0.05$ revealed, on heating in an applied field H_a, evidence for two magnetic phases with an upper $T_N = 120\,\mathrm{K}$ for $H_a \leqslant 100\,\mathrm{Oe}$, but only one magnetic ordering temperature $T_N = 100\,\mathrm{K}$ for $H_a \geqslant 800\,\mathrm{Oe}$. After a FC in 1 kOe, only the $T_N = 100\,\mathrm{K}$ was observed for all values of $H_a \leqslant 1$ kOe. (2) All ZFC samples exhibited M-H hysteresis loops at 10 K and 60 K that failed to saturate at high fields as is illustrated by the ZFC loop of Fig. 3. These first two observations are typical of spin-glass behavior, but the other two are not. (3) No M-H loop was displaced significantly along the field axis after cooling in 1 kOe. (4) The relaxation data were not typical of a spin glass. A ZFC spin glass would show, on application of an H_a, a long-time nonexponential increase in the magnetization M with time t and the relaxation rate $dM/d(\ln t)$ would show a broad maximum. Neither of these features was observed, as is illustrated in Fig. 6 for $x=0.05$.

The relaxation measurements were made at 10 K, well below T_a. The samples were held at 10 K in zero field for a waiting time t_w before a field $H_a = 100\,\mathrm{Oe}$ was applied at $t=0$. The magnetization was measured every 5 min for 14 h. Note that the magnitude of M with $t_w = 0.0\,\mathrm{h}$ was much

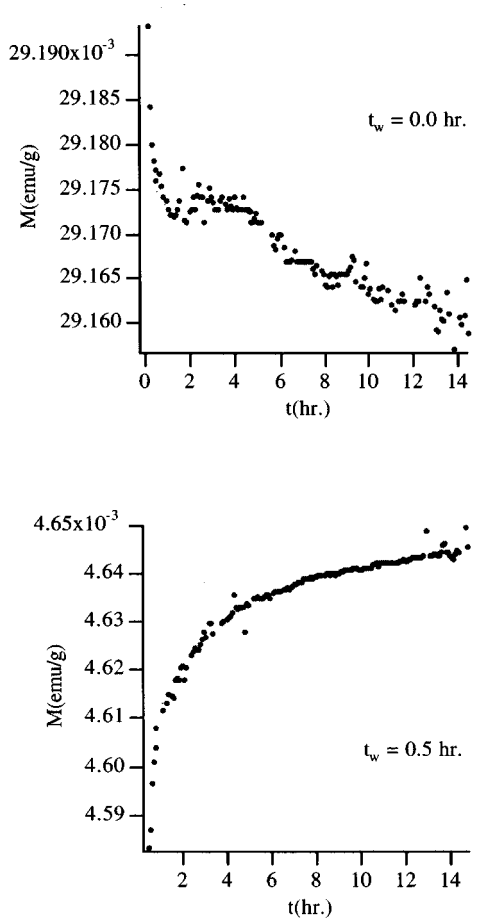

FIG. 6. Relaxation of magnetization for $La_{0.95}Sr_{0.05}TiO_3$.

larger than with $t_w = 0.50$ h. In fact, M decreased with increasing waiting time t_w in zero field, and M actually decayed with t in $H_a = 100$ Oe for $t_w = 0.0$ h.

C. Transport properties

The thermoelectric power $\alpha(T)$ (Fig. 7) and the resistance $R(T)$ (Fig. 8) show a change from polaronic p-type conduction for $x \leqslant 0.025$ to n-type metallic behavior at $x = 0.05$,

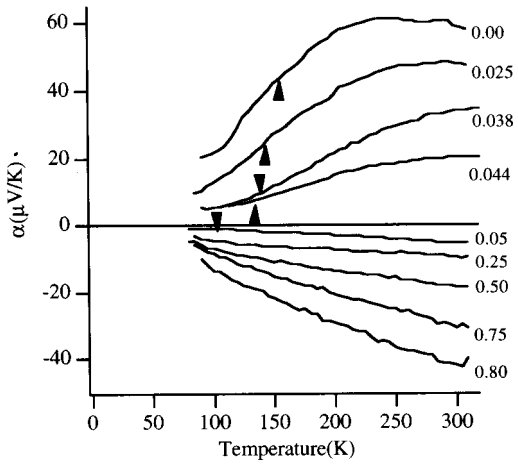

FIG. 7. Temperature dependence of the thermopower, $\alpha(T)$, vs x.

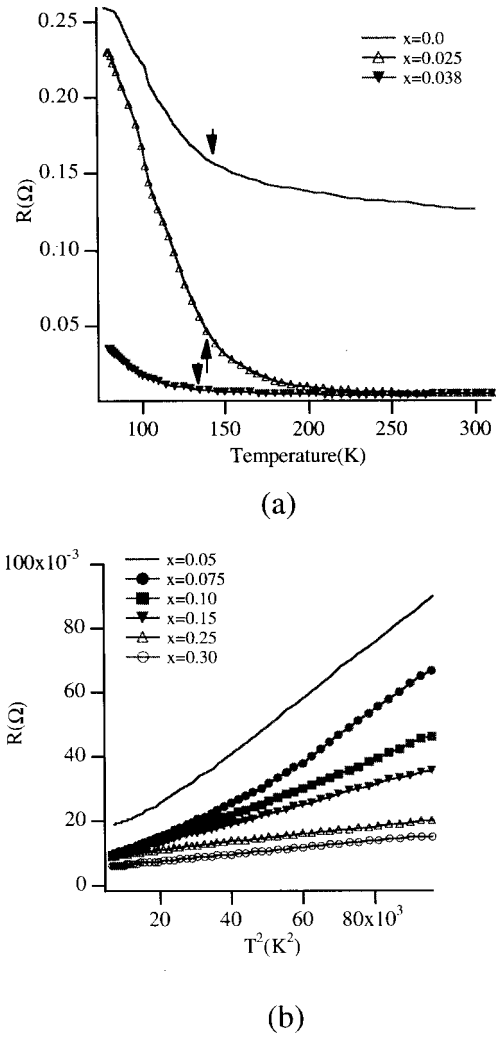

FIG. 8. Temperature dependence of resistance, $R(T)$, (a) for $x \leqslant 0.038$, and (b) for $0.05 \leqslant x \leqslant 0.30$.

where the Néel temperature T_N drops precipitously to 100 K. There is no anomaly in the transport data at T_N.

In the range $x \leqslant 0.025$, the resistance is well described by the expression $R = R_0 \exp(-E_a/k_B T)$ over the range $90 < T < 300$ K. The $x = 0$ sample had an $E_a = 0.08$ eV, which is typical for a small polaron mobility. On heating, the $R(T)$ curve for the $x = 0.038$ composition exhibits a smooth transition near 230 K from a semiconductive to a metallic temperature dependence; this transition suggests the onset of a percolation pathway at higher temperatures as an insulator-metal transition is approached. In fact, the $x = 0.044$ sample was already metallic even though it remained p type. The p-type conduction can only occur where an energy gap $E_g = (U - W) \geqslant 0$ is opened between the Ti^{4+}/Ti^{3+} and Ti^{3+}/Ti^{2+} redox couples and oxidation of the $(TiO_3)^{(3-\eta)-}$ array has lowered the Fermi energy ε_F into the narrow Ti^{4+}/Ti^{3+} band. As the character of the charge carriers changes from polaronic to itinerant, perturbation of the periodic potential by the Sr^{2+} ions or cation vacancies may transform the polaronic states into Anderson-localized states with variable-range hopping before ε_F falls below the mobility edge to give metallic behavior. Alternatively, a first-order polaronic to itinerant-electron transition would result in a phase segregation at crossover that, in the perovskite struc-

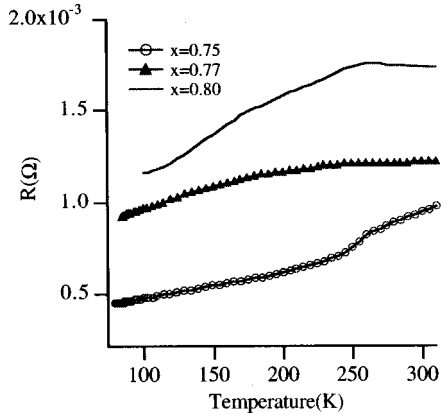

FIG. 9. Temperature dependence of resistance for $0.75 \leqslant x \leqslant 0.80$.

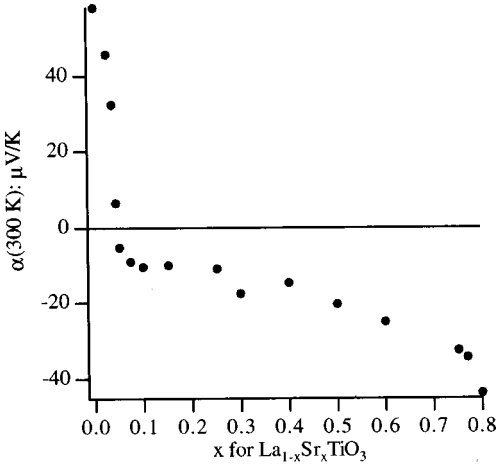

FIG. 10. Thermoelectric power at 300 K vs x.

ture, can be accomplished by cooperative oxygen displacements.[23] In this case, the volume of the minority itinerant-electron phase would increase as holes were thermally excited into it from the polaronic phase; above a critical temperature, the itinerant-electron phase would reach a percolation threshold.

The system becomes n type where $W > U$ closes the energy gap E_g. As has been reported, the metallic samples with $0.15 < x < 0.5$ are well described by the relation $R = R_0 + AT^2$, which is typical of electron-electron scattering in strongly correlated systems. In the range $0.05 \leqslant x \leqslant 0.15$, this relation holds above T_N and the coefficient A decreases progressively with increasing x, but there is a transition in the magnitude of A near 230 K for $0.075 \leqslant x \leqslant 0.15$.

The variation of volume with x in Fig. 1 indicates that the samples with $0.7 < x \leqslant 0.8$ have excess oxygen, which translates into cation vacancies. Cation vacancies would create a strong Coulombic repulsion for Ti-$3d$ electrons and, across a Ti vacancy, strong repulsion of the O^{2-} ions. An oxygen displacement away from the Ti vacancy would create a short Ti-O bond, which would stabilize the site t orbital perpendicular to the axis of the short Ti-O bond. Such a local bond ordering would become disordered at higher temperatures. Figure 9 shows a change in $R(T)$ near 250 K that may be related to such an orbital disordering in a system near a percolation threshold for transport via Ti atoms neighboring La^{3+} ions. A change in the sign of $dR(T)/dT$ in an $x = 0.80$ sample has been reported to occur at 190 K.[22]

By way of contrast, it is interesting to note that the $SrTiO_{3-\delta}$ perovskites become superconductive at lowest temperatures ($T_c < 0.3$ K) (Ref. 25) and that for large values of δ the samples are metallic and Pauli paramagnetic.[26] Doping by introducing oxygen vacancies does not trap the electrons at the vacancy whereas La^{3+} ions trap the electrons they introduce into the $3d$ bands of the TiO_3 array of $La_{1-x}Sr_xTiO_3$. In $SrTiO_{3-\delta}$, the titanium atoms on either side of an oxygen vacancy are displaced by the Coulomb repulsion between them to form short Ti(IV)-O bonds opposite to the vacancy, thereby releasing the electrons introduced to the matrix.

Both the $x = 0.044$ and $x = 0.05$ samples are antiferromagnetic and there is a change from p-type to n-type conduction on going from one to the other. Therefore, we chose to compare the change with hydrostatic pressure of their transport properties. Both samples remained metallic with both R_0 and A of the relation $R = R_0 + AT^2$ decreasing progressively under pressure. The lack of any anomaly at T_N prevented monitoring the change of T_N with pressure P. Figure 10 shows the dramatic decrease in the room-temperature thermoelectric power $\alpha(300\ \text{K})$ with increasing x in the range $0 < x < 0.05$. Figure 11(a) shows $\alpha(T)$ under different hydrostatic pressures for the $x = 0.044$ sample. Two points can be noted: (1) $\alpha(300\ \text{K})$ changes sign between 10 and 15 kbar and (2) what appears to be a weak phonon drag at low temperature is enhanced by pressure. The $\alpha(T)$ curves for $x = 0.05$ [Fig. 11(b)] show an $\alpha(300\ \text{K})$ that remains negative with a magnitude that increases to a saturation by 11.7 kbar, but there is no change in the phonon-drag component. An increase in $|\alpha(300\ \text{K})|$ with P is not characteristic of a conventional metal such as Pt, but it could indicate the transfer of spectral

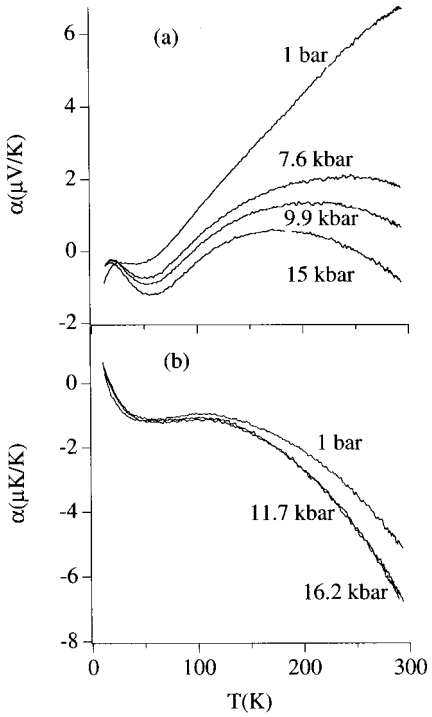

FIG. 11. Temperature dependence of thermopower, as a function of applied pressure for (a) $x = 0.044$ and (b) $x = 0.05$.

weight from incoherent to coherent occupied states as occurs in $CaVO_3$.[27] However, the $x=0.044$ sample is antiferromagnetic, and there is no evidence of a transfer of spectral weight below T_N. Fujimori *et al.*[9] have used photoemission spectroscopy to demonstrate the coexistence of coherent and incoherent states in $LaTiO_{3+\delta}$.

IV. SUMMARY AND CONCLUSION

The structural and magnetic data are consistent with an abrupt phase change at a crossover from an antiferromagnetic insulator to a strongly correlated metal in the interval $0.04<x<0.08$. The antiferromagnetic phase has a large spin canting suggestive of a large antisymmetric exchange associated with an unquenched orbital angular momentum. However, there is no evidence of a corresponding cooperative Jahn-Teller deformation below T_N that maximizes the orbital angular momentum as would be expected were the Ti-3*d* electrons localized. Nevertheless, at small x the charge carriers are small *p*-type polarons that, at low temperatures, become trapped at the Sr^{2+} ion and/or cation vacancies that introduced them.

In this mixed-valent system, the antiferromagnetic phase changes from a *p*-type small-polaron conductor for $x \leqslant 0.025$ to a *p*-type metal at $x=0.044$ before becoming an *n*-type metal for $x \geqslant 0.05$. Under hydrostatic pressure, the $x=0.044$ sample changes from a *p*-type to an *n*-type conductor. Across the transition from *p*-type polaron to *n*-type metal, the Néel temperature T_N drops precipitously to about 100 K, where it remains constant across a narrow two-phase domain $0.05 \leqslant x \leqslant 0.08$ where the net canted-spin moment decreases continuously with increasing x. This behavior would seem to demonstrate that the mixed-valent transition from polaronic to itnerant behavior may occur where the correlation gap $E_g=(U-W)>0$ is still retained. However, the absence of any anomaly in the temperature dependence of the transport properties at the Néel temperature T_N is unusual for itinerant electrons. This behavior seems to indicate that the itinerant carriers are associated with a separate, percolating metallic phase, which leads us to consider an electrically inhomogeneous model for the transition.

Independent evidence[9,27] for the coexistence of incoherent and coherent electronic states at the crossover from a magnetically ordered to a Pauli paramagnetic phase has been reported for oxides with the perovskite structure.[9,28] In the system $Sr_{1-x}Ca_xVO_3$, for example, the Brinkman-Rice[29] mass enhancement for a homogeneous electronic system breaks down where there is a coexistence of incoherent and coherent states within a phase with an enhanced Pauli paramagnetism and no long-range magnetic order.[27] We suggest that where the concentration of incoherent fluctuations becomes large enough, the fluctuations may interact to stabilize a phase with long-range antiferromagnetic order. On the approach to the transition from long-range antiferromagnetic order to short-range incoherent-electron fluctuations, we can envisage the onset of a percolating coherent-electron phase coexisting with a phase exhibiting long-range antiferromagnetic order. At this onset, T_N may drop precipitously to a finite value, but the canted-spin moment would decrease smoothly to zero as the volume of antiferromagnetic phase was diminished with increasing x. Our data are consistent with such an evolution at the crossover from long-range antiferromagnetic order in a *p*-type polaronic phase to an *n*-type metallic phase with a strongly enhanced Pauli paramagnetism.

In the perovskite structure, cooperative oxygen displacements are capable of separating the electronic system into two phases, and in this case, the phase boundaries may be mobile.[23]

Finally, the first-order character of the transition and the strong deviation from Végard's law in Fig. 1 follow Ref. 30 from the virial theorem for central-force fields,

$$2\langle T\rangle + \langle V\rangle = 0.$$

In the polaronic antiferromagnetic state, the electrons occupy a smaller volume and therefore have a larger mean kinetic energy, which requires the mean potential energy $|\langle V\rangle|$ to have a larger magnitude. It follows that the equilibrium Ti-O bond length is longer in the polaronic phase since the electrons occupy antibonding Ti-3*d* states. An increase in $\langle T\rangle$ with increasing electron correlations among itinerant electrons accounts for the significant deviation from Végard's law in Fig. 1, and a discontinuous change in $\langle T\rangle$ on crossing from polaronic to itinerant behavior requires a discontinuous change in the equilibrium Ti-O bond length to give a first-order phase change. Reedyk *et al.*[8] have reported a systematic increase with decreasing x in the Raman scattering rate, which they point out indicates the free-carrier scattering originates from changes in electronic structure as the electron-phonon coupling increases with the strength of the electron correlations in the range $0.1 \leqslant x \leqslant 0.5$.

ACKNOWLEGMENTS

We thank the National Science Foundation (Grant No. DMR 9528826 and No. DMR9705414) and the Robert A. Welch Foundation (Grant No. F-1191) for their support of this work.

*Present address: Dept. of Materials Science & Engineering, California Institute of Technology, Pasadena, CA 91125.

[1] J. B. Goodenough, Prog. Solid State Chem. **5**, 145 (1972).
[2] D. A. MacLean, H.-N. Ng, and J. E. Greedan, J. Solid State Chem. **30**, 35 (1979).
[3] C. W. Turner and J. E. Greedan, J. Solid State Chem. **34**, 207 (1980).
[4] J. P. Goral, J. E. Greedan, and D. A. MacLean, J. Solid State Chem. **43**, 244 (1982).
[5] J. E. Greedan, J. Less-Common Met. **14**, 335 (1985).
[6] D. A. Crandles, T. Timusk, J. D. Garrett, and J. E. Greedan, Phys. Rev. B **49**, 16 207 (1994).
[7] G. Amow and J. E. Greedan, J. Solid State Chem. **121**, 443 (1996).
[8] M. Reedyk, D. A. Crandles, M. Cardona, J. D. Garrett, and J. E. Greedan, Phys. Rev. B **55**, 1442 (1997).
[9] A. Fujimori, I. Hase, H. Namatame, Y. Fujishima, Y. Tokura, H. Eisaki, S. Uchida, K. Takegahara, and F. M. F. de Groot, Phys. Rev. Lett. **69**, 1796 (1992).
[10] Y. Tokura, J. Phys. Chem. Solids **53**, 1619 (1992).

[11] Y. Fujishima, Y. Tokura, T. Arima, and S. Uchida, Phys. Rev. B **46**, 11 167 (1992).
[12] Y. Taguchi, Y. Tokura, T. Arima, and F. Inaba, Phys. Rev. B **48**, 511 (1993).
[13] Y. Tokura, Y. Taguchi, Y. Okada, Y. Fujishima, T. Arima, K. Kumagai, and Y. Iye, Phys. Rev. Lett. **70**, 2126 (1993).
[14] Y. Okada, T. Arima, Y. Tokura, C. Murayama, and N. Mori, Phys. Rev. B **48**, 9677 (1993).
[15] K. Kumagai, T. Suzuki, Y. Taguchi, Y. Okada, Y. Fujishima, and Y. Tokura, Phys. Rev. B **48**, 7636 (1993).
[16] Y. Tokura, Phys. Rev. B **48**, 14 063 (1993).
[17] Y. Okimoto, T. Katsufuji, Y. Okada, T. Arima, and Y. Tokura, Phys. Rev. B **51**, 9581 (1995).
[18] T. Katsufuji, Y. Taguchi, and Y. Tokura, Phys. Rev. B **56**, 10 145 (1997).
[19] The arc furnace design is described in the Master's degree thesis of Charles C. Hays, Texas A&M University, 1986.
[20] J. B. Goodenough, J.-S. Zhou, and J. Chan, Phys. Rev. B **51**, 3104 (1995).
[21] M. Eitel and J. E. Greedan, J. Less-Common Met. **116**, 95 (1986).
[22] J. E. Sunstrom, IV, S. M. Kauzlarich, and P. Klavins, Chem. Mater. **4**, 346 (1992).
[23] J. B. Goodenough, Australian J. Phys. (to be published).
[24] C. C. Hays, Ph.D. thesis, University of Texas at Austin, 1997.
[25] C. S. Koonce, M. L. Cohen, J. F. Schooley, W. R. Hosler, and E. R. Pfeiffer, Phys. Rev. **163**, 380 (1967).
[26] W. Gong, H. Yun, Y. B. Ning, J. E. Greedan, W. R. Datars, and C. V. Stager, J. Solid State Chem. **90**, 320 (1991).
[27] J.-S. Zhou and J. B. Goodenough, Phys. Rev. B **54**, 13 393 (1996).
[28] I. H. Inoue, I. Hase, Y. Aiura, A. Fujimori, Y. Haruyarma, T. Maruyarna, and Y. Nishihara, Phys. Rev. Lett. **74**, 2539 (1995).
[29] W. F. Brinkman and T. M. Rice, Phys. Rev. B **2**, 4302 (1970).
[30] J. B. Goodenough, Ferroelectrics **130**, 77 (1992).